Journal of Marine Systems 76 (2009) 397–404

Contents lists available at ScienceDirect

Journal of Marine Systems

journal homepage: www.elsevier.com/locate/jmarsys

Internal tidal currents in the Gaoping (Kaoping) Submarine Canyon

I-Huan Lee [a], Yu-Huai Wang [b,*], James T. Liu [c], Wen-Ssn Chuang [d], Jingping Xu [e]

[a] National Museum of Marine Biology and Aquarium, Pingtung, Taiwan, 944-50, ROC
[b] Institute of Applied Marine Physics and Undersea Technology, National Sun Yat-sen University, Kaohsiung, Taiwan, 804-24, ROC
[c] Institute of Marine Geology and Chemistry, National Sun Yat-sen University, Kaohsiung, Taiwan, 804-24, ROC
[d] Institute of Oceanography, National Taiwan University, Taipei, Taiwan, 106-17, ROC
[e] U.S. Geological Survey (USGS), Santa Cruz and Menlo Park, CA95060, USA

ARTICLE INFO

Article history:
Received 1 October 2007
Revised 19 November 2007
Accepted 20 December 2007
Available online 31 August 2008

Keywords:
Gaoping (Kaoping) River
Submarine Canyon
Internal tidal currents
Standing wave

ABSTRACT

Data from five separate field experiments during 2000–2006 were used to study the internal tidal flow patterns in the Gaoping (formerly spelled Kaoping) Submarine Canyon. The internal tides are large with maximum interface displacements of about 200 m and maximum velocities of over 100cm/s. They are characterized by a first-mode velocity and density structure with zero crossing at about 100 m depth. In the lower layer, the currents increase with increasing depth. The density interface and the along-channel velocity are approximately 90° out-of-phase, suggesting a predominant standing wave pattern. However, partial reflection is indicated as there is a consistent phase advance between sea level and density interface along the canyon axis.

1. Introduction

Submarine canyons are common features on the continental shelves and margins. Their horizontal scales are small, on the order of several kilometers, but the vertical scales can be over 1000 m. The canyons often play the role of the conduit connecting the inner shelf to the deep ocean. The flow patterns in submarine canyons are complicated due to the complex topography. Klinck (1988) showed that a submarine canyon can be considered narrow if its width is less than about half of the internal Rossby deformation radius, O (10km) in mid-latitudes. In a narrow canyon, the water motion along the axis often is dominated by the tidal currents (Shepard et al., 1979). Studies have shown that the tides play the dominant role in driving the internal tides and internal waves and creating turbulence (Hotchkiss and Wunsch, 1982; Petruncio et al., 1998; García Lafuente et al., 1999; Carter and Gregg, 2002; Kunze et al., 2002; Xu et al., 2002; Liu et al., 2006).

The Gaoping (formerly spelled Kaoping) Submarine Canyon (KPSC) is a narrow submarine canyon off the southwest Taiwan. In recent years, several studies have been conducted in KPSC to study sediment transport processes (Liu et al., 2002; Liu and Lin, 2004; Liu et al., 2006). These studies concluded that the KPSC acts as a trap and conduit for particles of both terrestrial and marine origins. The spatial scale of KPSC is comparable to that of Monterey Canyon (U.S.) and La Línea Submarine Canyon (Spain). Flows in Monterey Canyon are dominated by the internal tides of amplitudes of about 20cm/s; the barotropic tidal currents are small about 5cm/s (Petruncio et al., 1998). Flows in La Línea Submarine Canyon also are dominated by the internal tides but with much larger amplitudes of about 50cm/s (García Lafuente et al., 1999). For comparison, flows in KPSC are even larger, over 70cm/s (Lee and Liu, 2006). The nature of internal tidal currents in KPSC has not been examined. Due to intense fishing activities and strong internal tidal currents, mooring operations in KPSC can be quite hazardous (Lee and Liu, 2006). In this study, observations from several anchor stations and current meter mooring are combined to describe the internal tidal currents in KPSC.

* Corresponding author. Tel.: +886 7 5252055; fax: +886 7 5255359.
E-mail addresses: ihlee@nmmba.gov.tw (I-H. Lee), yhwang@nsysu.edu.tw (Y.-H. Wang), james@nsysu.edu.tw (J.T. Liu), chuang@ntu.edu.tw (W.-S. Chuang), jpx@usgs.gov (J. Xu).

0924-7963/$ – see front matter © 2008 Elsevier B.V. All rights reserved.
doi:10.1016/j.jmarsys.2007.12.011

2. Study area

The head of KPSC, off Donggang (Formerly spelled Tung-kang) (TK) harbor, is about 1km wide (Fig. 1). The mouth of the canyon is open to the northeast side of the South China Sea basin. The average width of KPSC is about 2–3km. The detailed topography has been documented by Liu et al. (2002), Liu and Lin (2004) and Liu et al. (2006). A notable characteristic of KPSC is the "S" shaped orientation of the canyon axis in the head. The canyon axis is oriented in the N–S direction near the head and turns sharply to the E–W direction about 10km down the canyon head. There is also a small Island, Siaoliuciou (Formerly spelled Hsiao-liu-chiu) (HLC), located at the southern bank of KPSC (Fig. 1).

3. Methods

Table 1 lists the data source from the five experiments used in this study. Locations of ship anchor and mooring for each experiment are shown in Fig. 1. Sea level data were from HLC. In the following, u and v represent the east- and northward velocity components. For experiments 1 and 5, the channel is orientated in the N–S direction, and for experiments 2 and 4 the channel is orientated in the E–W direction.

Table 1
Information for the five experiments

Exp	Date	Instrument	Observation depth of flow (water depth)	Parameters measured	Temporal/ spatial resolution
1	Jun. 28–Jul. 21, 2000	2 RCM8 current meters	200 m and 270 m (300 m)	*u*, *v*, *T*, *p*	1 h
2	Feb. 26–Feb. 27, 2004	sbADCP CTD	8 m– 320 m 0 m–350 m (410 m)	*u*, *v* *T*, *S*, *p*	2 min/8 m 1 h/1 m
3	May 26–Jun. 27, 2004	NADCM	240 m (315 m)	*u*, *v*, *T*, *p*	1 h
4	Dec. 13–Dec. 14, 2004	sbADCP btADCP CTD	8 m– 280 m 100 m–320 m 0 m–420 m (440 m)	*u*, *v* *u*, *v* *T*, *S*, *p*	30 s/8 m 5 min/2 m 1 h/1 m
5	Aug. 27–Aug. 28, 2006	btADCP CTD	87 m– 247 m 0 m–250 m (270 m)	*u*, *v* *T*, *S*, *p*	1 min/8 m 1 h/1 m

u, *v*: *x*- and *y*-components of flow; *T*: temperature; *p*: pressure; *S*: salinity. sbADCP: shipboard ADCP; btADCP: bottom-mounted ADCP; NADCM: Nortek Aquadopp Doppler current meter.

3.1. Experiment one (Exp1): time series of two current meters on a taut-line mooring

Experiment 1 was from June 20 to July 21, 2000 (Liu and Lin, 2004). Two RCM8s were installed on a mooring array near the bottom. The current meter depths were around 160 m and 195m at the beginning. However, the readings of the pressure sensors from the two RCM8s showed that the mooring array was moved to deeper depths for some unknown reason. The two RCM8s eventually settled after June 28 at about 200 m and 270 m depths, respectively. Only the data afterwards (about 20days) were used in the analysis. The eventual water depth was 320 m.

3.2. Experiment two (Exp2): 29-hour anchor station for hourly CTD and shipboard ADCP observations

Experiment 2 was in February 26–27, 2004. During the study, R/V Ocean Research I was kept in almost stationary position with a drifting radius of less than 1km. The local water depth was 410 m. The ADCP data were processed under the

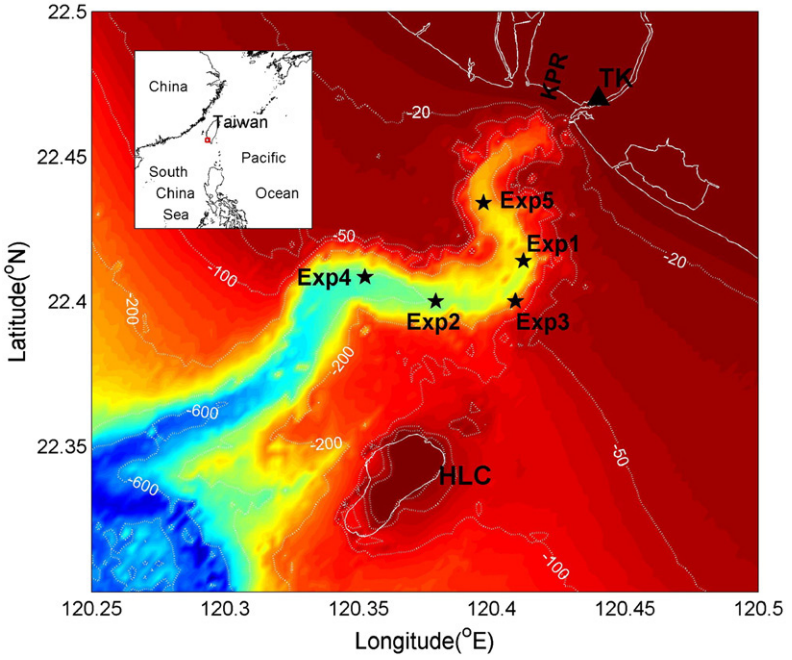

Fig. 1. Topography of Gaoping Submarine Canyon (m). The locations of each experiment (★), Siaoliuciou (formerly spelled Hsiao-liu-chiu) Island (HLC), Donggang (formerly spelled Tung-kang, TK) and Gaoping River (KPR) are marked.

standard data quality control (Wang et al., 2004). Because of the range limit of the shipboard ADCP, only 3/4 of the water column was sampled (8–320 m). The raw data resolution was 8 m in depth and every 2min in time. The data were averaged to generate hourly values at 8 m resolution. Between 8 and 248 m the data were intact, and between 256 and 320 m about 14% of data were extrapolated using cubic spline interpolation.

3.3. Experiment three (Exp3): time series of one current meter on a taut-line mooring

Experiment 3 was conducted in May 25–June 26, 2004. Two Nortek Aquadopp Doppler current meters (NADCMs) were installed on two mooring arrays. The configurations of these two moorings were described in Lee and Liu (2006). One current meter was at 50 m depth and the other at 235m. Both moorings however experienced severe tilt (Lee and Liu, 2006), which complicated the data processing. Experiment 3 therefore was not included in this study.

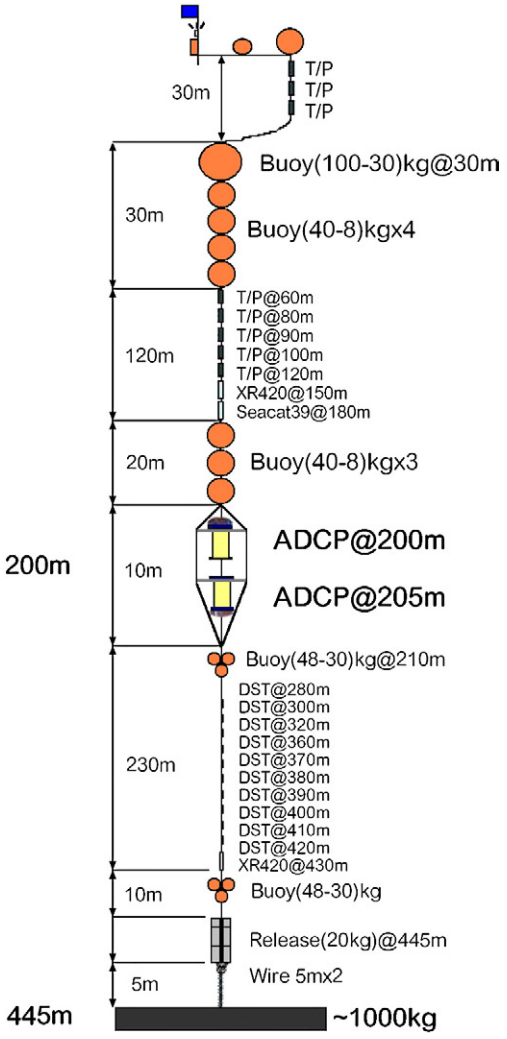

Fig. 2. Mooring configuration for Experiment 4. Only data from two moored ADCPs are used in this study.

3.4. Experiment four (Exp4): time series of two ADCPS on a taut-line mooring

Experiment 4 was from December 13 to 20, 2004. The mooring was located about 2km to the west of Exp2. The water depth was 440 m. The mooring configuration is shown in Fig. 2. Only data from the two 300kh Workhourse ADCPs were used in this study. These two ADCPs were installed on the mooring array in the middle of the water column at 200 m, one upward-looking and the other downward-looking. The raw data resolution was 2m in depth and every 5min in time, and the depth range for each ADCP was about 150 m. During the observations, the mooring was affected by strong tidal currents with significant vertical excursions of about 50 m. The data quality though is good because the two instruments always stayed vertical. The data were averaged into 10 m vertical resolution every hour. The combined ADCP data covered the depth range between 110 and 320 m.

The CTD and shipboard ADCP data were collected in the first 18h of Exp4. The shipboard ADCP data were calibrated and merged with mooring ADCP data.

3.5. Experiment five (Exp5): time series of bottom-mounted ADCP measurements

Experiment 5 was in August 27–28, 2006. The location was near the head of the canyon. The local water depth was 270 m. The data included bottom-mounted ADCP and hourly CTD observations. The resolution of the raw ADCP data was 8 m in depth and 1min in time. The ADCP data were averaged into 8 m vertical resolution every 10 min, and the depth range was between 87 and 247 m.

4. Results

4.1. Experiment 1

Fig. 3 shows records from the two RCM8s of Exp1 (Fig. 3a–d) and the corresponding sea levels at HLC (Fig. 3e). The pressure records indicate that the two RCM8s are stable with small depth-fluctuations. The flows in v-direction mainly reflect the along-channel motion; the positive v is up-canyon. The velocity amplitudes are larger at 270 m than that at 200 m, suggesting that the flows increase with depth. Fig. 4 shows power spectra of velocity and temperature (at 200 m) and coherence and phase between velocity, temperature and sea level. Both the velocity and temperature fluctuations are dominated by the semi-diurnal tides; though, the diurnal and higher-harmonics also are significant. The sea level fluctuations, on the other hand, have comparable diurnal and semi-diurnal constituents. Harmonic analysis indicates that the major tidal constituents are S_2 (0.14 m), M_2 (0.28 m), K_1 (0.28 m), and O_1 (0.21m). These four major constituents account for 90% of the observed variance.

The velocity, temperature and sea level fluctuations are highly coherent at the semi-diurnal period (Fig. 4). The phase between velocity and temperature is 110°, that is, temperature minimum leads the slack water after flood current, by about an hour. “Flood current” is used in the text to mean up-canyon flow in the lower water column. The nearly

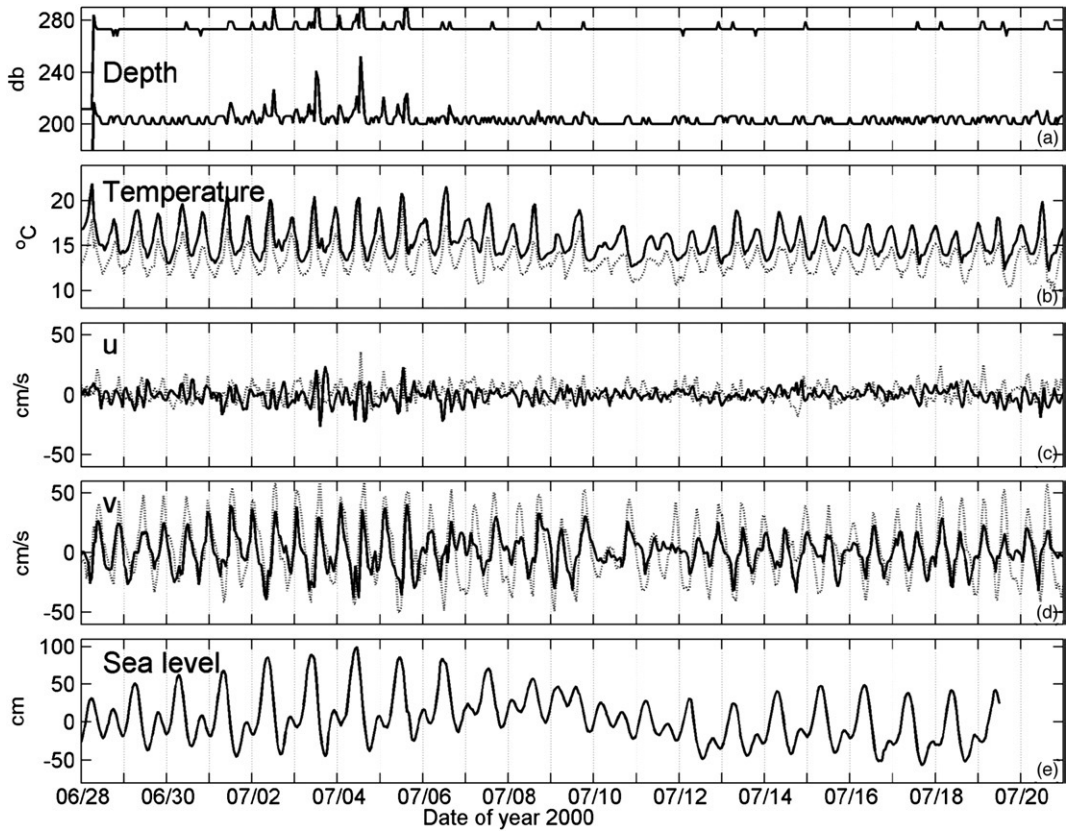

Fig. 3. Pressure (a), temperature (b), and velocity (c–d) from two RCM8s at 200 m (solid lines) and 270 m (dashed lines) of Experiment 1, and sea level at HLC (e).

90° phase relationship is characteristic of a standing wave. The phase between velocity (temperature) and sea level is 140° (30°); or, the low water leads the temperature minimum by about an hour. We note that the velocity and temperature fluctuations are coherent at the diurnal and quarter-diurnal periods too.

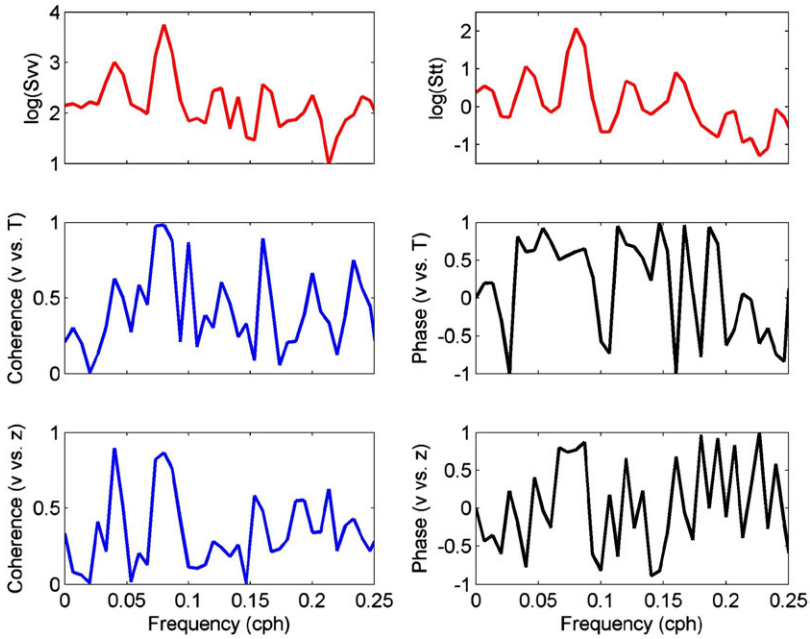

Fig. 4. Cross-spectrum of along-channel velocity component (v) vs. temperature (T) and sea level for current meter at 200 m. Shown are spectrum of v (Svv) and T (Stt), and coherence and phase (in unit of π) between v and T (v vs. T), and between v and HLC sea level (v vs. z).

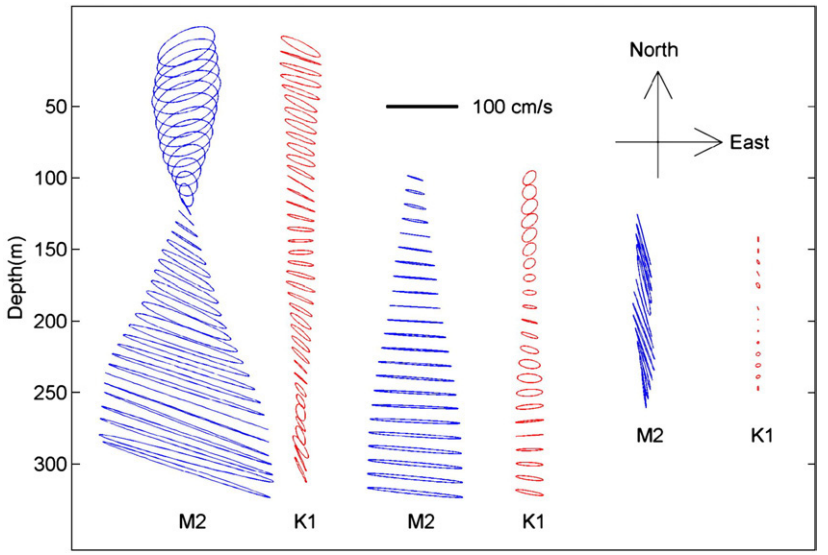

Fig. 5. Tidal ellipses of semi-diurnal (M_2) and diurnal (K_1) tidal currents for Experiment 2 (left), Experiment 4 (middle) and Experiment 5 (right).

4.2. Experiment 2

The data include 29h of shipboard ADCP and CTD observations. The axis of KPSC at this location is oriented E–W. Fig. 5 shows the tidal ellipses of semi-diurnal (M_2) and diurnal (K_1) tide. The M_2 is much larger than K_1, which agrees with the spectral results in Exp1. The K_1 decreases gradually with depth. The M_2, on the other hand, has a distinct baroclinic (first-mode) structure with zero crossing at about 120 m. The M_2 velocity increases towards the bottom, which also agrees with the findings in Exp1 (note that the local water depth is 410 m). Fig. 6 shows the time series of velocity vectors plotted over corresponding density contours; the semi-diurnal component of the sea level is superimposed. The velocity and density are about 90° out-of-phase, that is, the density maximum occurs at the end of the flood current. While the record is too short to establish a precise phase relation, the approximate 1h (30°) offset between the density maximum (temperature minimum) and slack water (after flood) agrees well with Exp1. The low water leads the density maximum by about 3h.

4.3. Experiment 4

Fig. 5 shows the tidal ellipses of M_2 and K_1 between 100 and 320 m from the 7-day moored ADCP observations. The M_2 tidal ellipses are similar at comparable depths to those of Exp2; the zero crossing is slightly shallower. Fig. 7 shows the along-

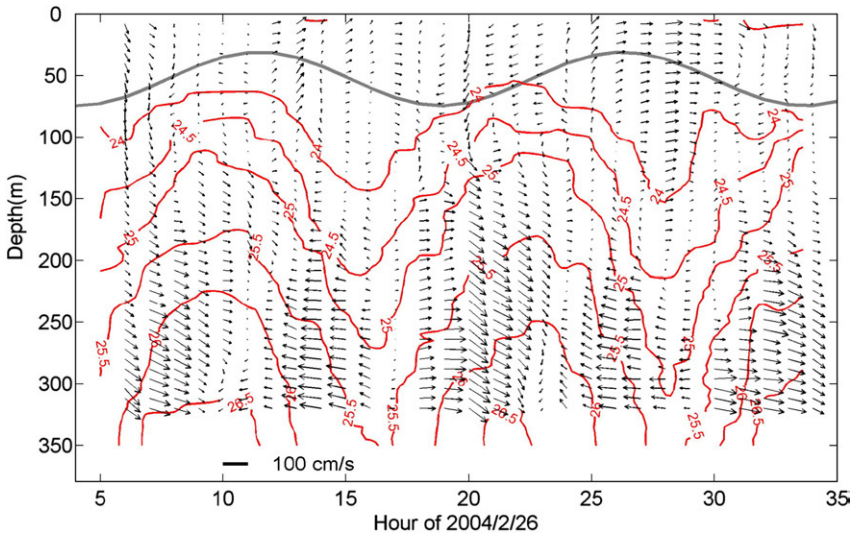

Fig. 6. Time series of flow vectors plotted over density variations for Experiment 2. Sea level (exaggerated) at HLC (M_2 tide only) is marked for reference (gray line). Arrows indicate positive flow in East-North coordinate system.

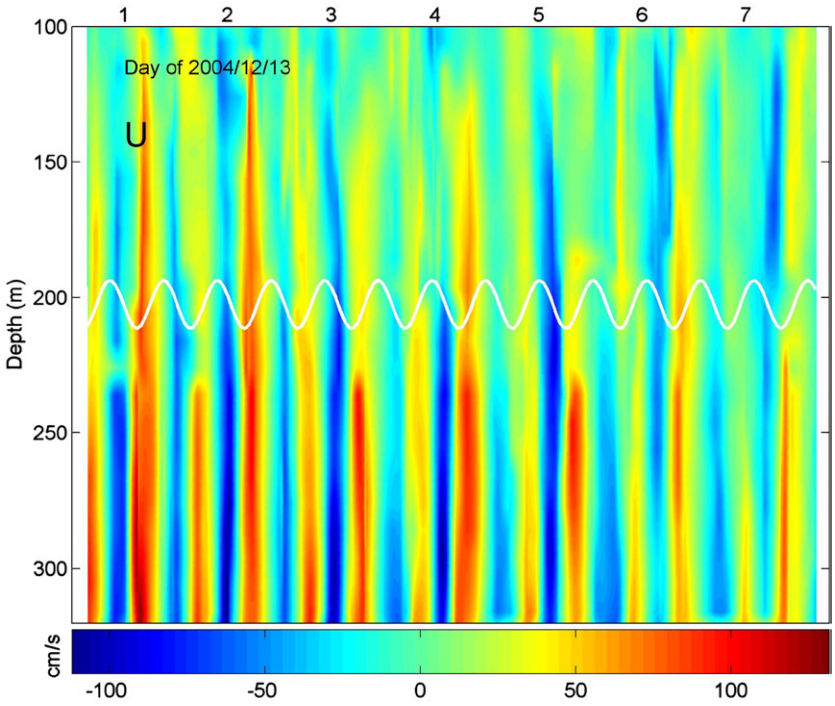

Fig. 7. Time series of along-channel velocity component from combined shipboard and mooring ADCP data. HLC sea level variation (thick line, M_2 tide only) is marked for reference.

channel velocity from the ADCP data with corresponding semi-diurnal component of the sea level. In general, the rising sea level corresponds to the flood current. Fig. 8 shows 18-hour combined ADCP velocity vectors and density contours from the anchor station. The results are similar to Exp2 in that the density maximum occurs at the end of the flood current and the density minimum at the end of the ebb current. The relation between density and sea level also agrees with Exp2.

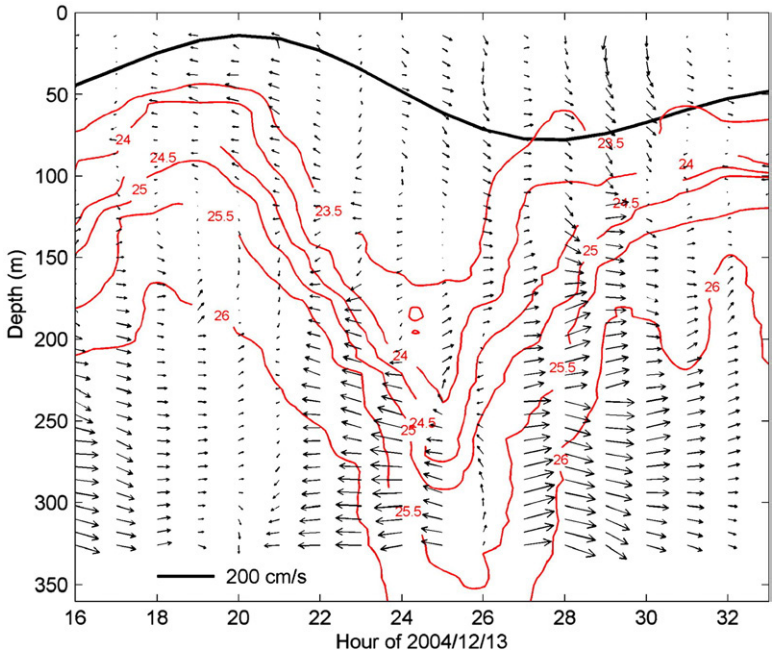

Fig. 8. Time series of flow vectors plotted over density variations for Experiment 4. Sea level variation of HLC is marked for reference (M_2 tide only). Arrows indicate positive flow to the east (u) and north (v) directions.

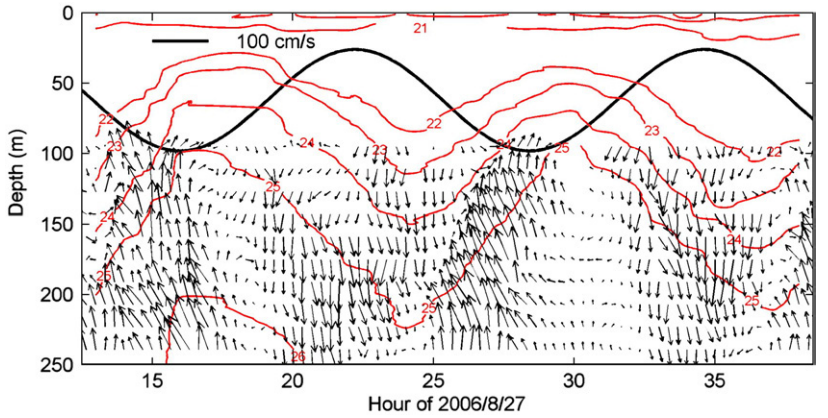

Fig. 9. Time series of flow vectors plotted over density variations for Experiment 5. Sea level variation of HLC is marked for reference (M_2 tide only). Arrows indicate positive flow in East-North coordinate system.

4.4. Experiment 5

Fig. 5 shows the tidal ellipses of M_2 and K_1 between 140 and 250 m from the 23-hour bottom-mounted ADCP observations. The M_2 is almost uniform, indicating that the measurement is completely in the lower layer. Fig. 9 shows combined velocity vectors and density contours. The density maximum occurs at the end of the flood current and the density minimum at the end of the ebb current. These results are similar to all the other experiments. The approximate 1-hour phase difference between sea level and density agrees with the 30° phase found in Exp1.

5. Discussion and summary

Five field experiments in KPSC were carried out from 2000 to 2006. Despite the differences in location and time, the results indicate a consistent picture of the semi-diurnal internal tides that can be described approximately as a first-mode standing wave with velocity and density interface about 90° out-of-phase. Similar standing internal tides were reported at the Upper Loch Linnhe of Scotland (Allen and Simpson, 1998) and at the outer continental slope of northern California (McPhee-Shaw et al., 2004). It should be noted that partial reflection of internal tides is likely as intense dissipation is expected near the canyon head. The present study does not permit examination of the phase propagation. However, if we use semi-diurnal sea level as a reference, it is possible to obtain an estimate of the along-canyon phase change. For Exp1 (Fig. 4) and Exp5 (Fig. 9) the low water leads the density maximum by about an hour. For Exp2 (Fig. 6) and Exp4 (Fig. 8), on the other hand, the low water leads the density maximum by about 3–4h. Thus, despite the short records, there appears to be a consistent phase advance of about 3h between the main channel and the canyon head. Assuming a phase speed of 1.2m/s (based on the mean vertical density profile) for the first-mode internal tide, the estimated wavelength is about 50km. The estimated 3-hour phase difference is indeed consistent with the expected quarter-wavelength phase difference between the main channel and the canyon head. Future studies with synchronized along-canyon survey are needed to examine the inferred phase propagation. Also, it will be useful to extend the observations to the mouth of the canyon to study the generation processes.

The large internal tidal flows likely have major impact on the material transport in the Gaoping Canyon. Hung and Hsu (2004) indicated that the Gaoping Canyon acted as a major sink for river borne trace metals. Jeng et al. (1996) found that the coprostanol concentration was highest at the river mouth but remained high at 35km from the canyon head. It appears that the oscillating internal tidal currents provide effective mixing of sediments along the Gaoping canyon. We note that the velocity measurements typically did not reach the bottom. From the perspective of sediment transport, it would be desirable to obtain in the future the velocity measurements in the lowest 100 m.

Acknowledgements

We appreciated comments from two reviewers to improve the manuscript. Dr. Dong-ping Wang provided helpful discussions. The funding for this study was provided by the ROC National Science Council (NSC) under grant numbers: NSC91-2611-M-110-017, NSC92-2611-M-110-012, NSC93-2611-M-110-013, NSC94-2611-M-110-002 to J.T. Liu. YHW acknowledged partial supports from NSC (95-2611-M-110-014) and the Aim for Top University Plan.

References

Allen, G.L., Simpson, J.H., 1998. Reflection of the internal tide in Upper Loch Linnhe, a Scottish fjord. Estuar. Coast. Shelf Sci. 46, 683–701.
Carter, G.S., Gregg, M.C., 2002. Intense, variable mixing near the head of Monterey Submarine Canyon. J. Phys. Oceanogr. 32, 3145–3165.
García Lafuente, J., Sarhan, T., Vargas, M., Vargas, J.M., Plaza, F., 1999. Tidal motions and tidally induced fluxes through La Línea submarine canyon, western Alboran Sea. J. Geophys. Res. 104 (C2), 3109-3119.
Hotchkiss, F.S., Wunsch, C., 1982. Internal waves in Hudson canyon with possible geological implications. Deep-Sea Res. 29 (4A), 415–442.
Hung, J.J., Hsu, C.L., 2004. Present state and historical changes of trace metal pollution in Gaoping coastal sediments, southwestern Taiwan. Mar. Pollut. Bull. 49, 986–998.
Jeng, W.L., Wang, J., Han, B.C., 1996. Coprotanol distribution in marine sediments off Southwestern Taiwan. Environ. Pollut. 94 (1), 47–52.
Klinck, J.M., 1988. The influence of a narrow transverse canyon on initially geostrophic flow. J. Geophys. Res. 93 (C1), 509–515.
Kunze, E., Rosenfeld, L.K., Carter, G.S., Gregg, M.C., 2002. Inter waves in Monterey Submarine Canyon. J. Phys. Oceanogr. 32, 1890–1913.

Lee, I-H., Liu, J.T., 2006. Rectification of the heading and tilting of sediment trap arrays due to strong tidal currents in a submarine canyon. Geophys. Res. Lett. 33, L08609. doi:10.1029/2005GL025183.
Liu, J.T., Lin, H.L., 2004. Sediment dynamics in a submarine canyon: a case of river–sea interaction. Mar. Geol. 207, 55–81.
Liu, J.T., Lin, H.L., Hung, J.J., 2006. A submarine canyon conduit under typhoon conditions off Southern Taiwan. Deep-Sea Res. 53, 223–240.
Liu, J.T., Liu, K.J., Huang, J.C., 2002. The effect of a submarine canyon on the river sediment dispersal and inner shelf sediment movements in southern Taiwan. Mar. Geol. 181, 367–386.
McPhee-Shaw, E.E., Sternberg, R.W., Mullenbach, B., Ogston, A.S., 2004. Observations of intermediate nepheloid layers on the northern California continental margin. Cont. Shelf Res. 24, 693–720.
Petruncio, E.T., Rosenfeld, L.K., Paduan, J.D., 1998. Observations of the internal tide in Monterey Canyon. J. Phys. Oceanogr. 28, 1873–1903.
Shepard, F.P., Marshall, N.F., McLoughlin, P.A., Sullivan, G.G., 1979. Currents in submarine canyons and other sea valleys. AAPG Stud. Geol. 8 173pp.
Wang, Y.H., Chiao, L.Y., Lwiza, K.M.M., Wang, D.P., 2004. Analysis of flow at the gate of Taiwan strait. J. Geophys. Res. 109, C02025. doi:10.1029/2003JC001937.
Xu, J.P., Noble, M., Eittreim, S.L., Rosenfeld, L.K., Schwing, F.B., Pilskaln, C.H., 2002. Distribution and transport of suspended particulate matter in Monterey Canyon, California. Mar. Geol. 181, 215–234.